ACS OMEGA

http://pubs.acs.org/journal/acsodf

Article

Comparative and Selective Interaction of Amino Acid D-Cysteine with Colloidal Gold Nanoparticles in the Presence of a Fluorescent Probe in Aqueous Medium

Pradip Maiti, Ujjal Saren, Utsav Chakraborty, Tanmoy Singha, Sharmistha Paul, and Pabitra Kumar Paul*

Cite This: *ACS Omega* 2022, 7, 29013−29026

Read Online

ACCESS | Metrics & More | Article Recommendations | Supporting Information

ABSTRACT: In this communication, we report the comparative and selective interaction of amino acid D-cysteine (D-Cys) with citrate caped gold nanoparticles (Au NPs) in the presence of a fluorescent dye, rhodamine B (RhB), in aqueous solution. Au NPs of size 27.5 nm could almost fully quench the steady-state fluorescence emission of RhB at their optimum concentrations in the mixed solution. The interactions of D-Cys, L-Cys, all other relevant D- and L-amino acids, neurotransmitters, and other relevant biological compounds with the Au NPs/RhB mixed solution have been explored by monitoring the fluorescence recovery efficiencies from the almost fully quenched state of RhB fluorescence via a simple steady-state spectrofluorometric method. The higher fluorescence recovery for the interaction of D-Cys with the Au NPs/RhB mixed system is accompanied by a distinct color change (red-wine to bluish-black) of the assay medium after the reaction compared to that of all other interfering compounds considered in this work. The sensitivity of this fluorometric response lies in a broad linear range of concentrations of D-Cys and the limit of detection (LOD) is found to be 4.2 nM, which is low compared to many other methods available in the literature. The different degrees of interaction of D-Cys and L-Cys with the Au NPs/RhB mixed sample have been further explored by circular dichroism (CD) spectroscopy and Fourier transform infrared (FTIR) spectroscopy. The selective interaction of D-Cys with the proposed Au NPs/RhB mixed system is also found to be correlated with interparticle cross-linking and aggregations of nanoparticles by the analysis of ζ potential and dynamic light scattering (DLS) study, transmission electron microscopy (TEM), atomic force microscopy (AFM), UV−vis absorption spectroscopy etc. The proposed interaction mechanism is further studied with a normal human urine sample to elucidate that the optimized combination of Au NPs and RhB may be realized as an efficient platform for detection of the amino acid D-Cys in a real biosample via a simple fluorometric approach.

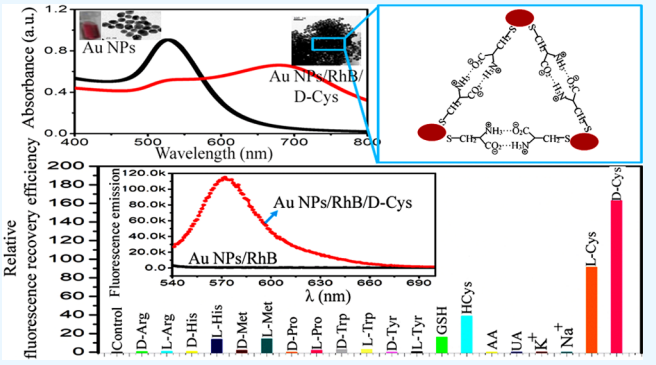

1. INTRODUCTION

The fundamental part of antibodies, signaling molecules, enzymes, hormones, receptors, and protein structures present in all living organisms is amino acids. They also act as biochemical rulers in the neurotransmission.[1,2] All of the amino acids present in the nature exist mainly in two forms: dextrorotatory (D) and levorotatory (L) enantiomers. On the basis of the protein-creating efficiency, there are in total 20 amino acids that have been reported. Previously, it was presumed that only L-amino acids were necessary in mammals, including humans, in the formation of components for proteins and peptides. However, various sensitive and selective analytical approaches developed for detecting chiral amino acids[3,4] suggested that diverse D-amino acids are also present in mammalian tissues. Different studies have been performed to explore the physiological functions of D-amino acids. The physiological and the biochemical activities of different D-amino acids such as D-cysteine (D-Cys), D-aspartate (D-Asp), D-alanine (D-Alan), D-serine (D-Ser) etc. in our nerve cells, skin, arterial walls, bones, other tissues, and body fluids, including amniotic fluid, urine, blood plasma, cerebrospinal fluid (CSF), saliva etc., have been systematically studied by various researchers in the last several years.[5,6]

The semi-essential, proteinogenic amino acid cysteine ($C_3H_7NO_2S$) (abbreviated as Cys) contains thiol (−SH), amine ($-NH_2$), and carboxylic (−COOH) functional groups.

Received: May 2, 2022
Accepted: August 1, 2022
Published: August 12, 2022

The −SH moiety mainly takes part in the nucleophilic enzymatic reactions.[7] Also, the −SH group plays an important structural role in the formation of many proteins by creating the disulfide derivative of Cys.[8] D-Cys creates hydrogen sulfide (H_2S) and decreases the disulfide bonds present in the receptors.[8] This may act synergistically and increase the responsiveness of neurotransmitters specifically to a particular activity. The deviant activity of receptors causes diseases in the central nervous system (CNS) such as amyotrophic lateral sclerosis, Alzheimer's disease, schizophrenia etc.[9,10] In the endocrine gland, H_2S prevents discharge of insulin due to glucose generation by the pernicious β cells.[11] Tong et al. showed that the biofilm formation of *Streptococcus mutans* and *Streptococcus sanguinis* on the surface of teeth could be controlled by free D-Cys.[12]

In recent times, the study of the interactions of various proteins and amino acids with nanoparticles (NPs) has attracted great attention in the field of nano-biotechnology.[13] Among the various amino acids, D-Cys is also responsible for the growth of various diseases and disorders in the human body. Thus, the selective and quantitative recognition of D-Cys is very important for the diagnosis and treatments of various diseases. D-Cys can interact and be functionalized with several interesting metal nanoparticles (NPs)[13,14] because NPs possess significant adsorption capabilities due to their large surface area to volume ratio.[15] Sometimes this type of biomolecules can bind with such NPs via selective covalent interactions.[16] Among the various metal-based NPs,[17,18] noble metal NPs such as gold nanoparticles (Au NPs) show significant prospects regarding their potential in various fields of biomedical applications such as drug delivery,[19] biomolecular sensing[20−22] etc. The high extinction coefficient of Au NPs in the visible region renders them as an efficient platform for signaling molecular recognition processes through their color change.[21] The small sizes of these metal NPs with a large surface curvature facilitate their binding with various organic dyes, proteins[16,18] etc. The degree of structural perturbation of the protein molecules due to their interaction with NPs varies for different protein species.[23] As the amino acids are the basic structural units of protein molecules, the study of the interaction of amino acids with Au NPs via a simple spectrofluorometric technique is of particular importance. The −SH-containing amino acid D-Cys is recognized as an important regulator of neurotransmitters and the overall neural cell dynamics in our physiological system. Therefore, a comparative study of the interaction of various forms of Cys and their chiral discrimination while interacting with Au NPs is important for both fundamental and biomedical interests.

In the present study, we have addressed the interaction or reactivities of D-Cys and L-Cys as well as all other relevant amino acids, neurotransmitters etc. with citrate caped Au NPs in the presence of a fluorescent probe, namely rhodamine B (RhB), in aqueous medium. RhB is a cationic organic dye with a high fluorescence quantum yield and has been used as an interesting signaling agent for various biomolecular recognition events.[24,25] The fluorescence emission of the RhB dye is almost fully quenched by the colloidal solution of Au NPs and the mechanism of the quenching has been described in detail in this work. The fully quenched fluorescence emission of this dye due to Au NPs in the aqueous solution is recovered via selective interaction with the amino acid D-Cys through SH−Au bond formation and aggregation of Au NPs. This interaction is also reflected as a distinct color change of the assay medium from red-wine to bluish-black, which is different from the interaction with L-Cys or any other interfering compounds studied in this work. The ratio-metric determination of the fluorescence recovery efficiency[26,27] in the presence of various analytes in the assay medium automatically eliminates the perturbation from any external influences during the assay. However, there are few recent reports on the detection of D-Cys based on various methods such as SRM-chromatography, colorimetric, ultra-high-performance liquid chromatography (UHPLC)-URMS-chromatography, electrokinetic chromatography etc.[28−32] However, the proposed fluorometric method, which is free from any direct leveling, offers great advantages for the detection of D-Cys, especially up to the nanomolar level. The aggregations of the Au NPs/RhB system in the presence of both the −SH-containing amino acids, D- and L-Cys, have been visualized by transmission electron microscopy (TEM) and atomic force microscopic (AFM) studies and are correlated with the observed Fourier transform infrared (FTIR), UV−vis absorption, and steady-state fluorescence spectroscopic results. The different extents of interaction of D-Cys and L-Cys with the proposed Au NPs/RhB mixed system in aqueous medium are also distinguished by the chiral properties using the circular dichroism (CD) spectroscopic technique. Au NPs and the RhB-based fluorescence turn-on sensing platform are also tested with normal human (male) urine as a real biosample to realize the same selective response of the D-Cys present in urine.

2. EXPERIMENTAL SECTION

2.1. Materials. All of the chemicals used in this work were of analytical grade and were used as obtained without further purification. Gold(III) chloride acid trihydrate ($HAuCl_4 \cdot 3H_2O$, MW: 393.83 g mol^{-1}), RhB ($C_{28}H_{31}ClN_2O_3$, MW: 479.02 g mol^{-1}), D-Cys ($C_3H_7NO_2S$, MW: 121.15 g mol^{-1}), and other D- and L-amino acids, ascorbic acid (AA) ($C_6H_8O_6$, MW: 176.12 g mol^{-1}), uric acid (UA) ($C_5H_4N_4O_3$, MW: 168.11 g mol^{-1}), glutathione (GSH) ($C_{10}H_{17}N_3O_6S$, MW: 307.33 g mol^{-1}), and homocysteine ($C_4H_9NO_2S$, MW: 138.18 g mol^{-1}) (Hcys), were purchased from Sigma-Aldrich Chemical Company. Trisodium citrate ($Na_3C_6H_5O_7$, MW: 258.06 g mol^{-1}), sodium chloride (NaCl, MW: 58.44 g mol^{-1}), and potassium chloride (KCl, MW: 74.5513 g mol^{-1}) were purchased from Merck Chemical Company, Germany. All of the glasswares were cleaned with freshly prepared aqua regia (mixture of HCl and HNO_3 in 3:1 ratio) followed by subsequent rinsing with triple distilled deionized Milli-Q water (resistivity 18.2 MΩ cm, pH ∼ 7 at 25 °C, collected from Synergy integrated with an Elix Advantage setup; make: Millipore SAS, France) and then were autoclaved for 24 h before use. Aqueous solutions of the samples were also prepared with the same triple distilled deionized Milli-Q water.

2.2. Synthesis of Au NPs. The well-documented Frens' soft chemical reduction method has been used to obtain monodispersed gold nanocolloids with the desired particle size distribution.[21,33] In brief, an aliquot of a 50 mL aqueous solution of $HAuCl_4 \cdot 3H_2O$ (0.25 M) was heated to boil and 1.2 mL of $Na_3C_6H_5O_7$ (1%) was added into the solution under vigorous stirring for the formation of gold nanocolloids. In about 100 s, the boiling solution turned faintly blue. After 120 s, the blue color changed to deep red, which indicates the formation of the spherical Au NPs. The synthesized nanocolloidal solution was set aside to cool down to room temperature and stored at 4 °C for future use. The final

https://doi.org/10.1021/acsomega.2c02725
ACS Omega 2022, 7, 29013−29026

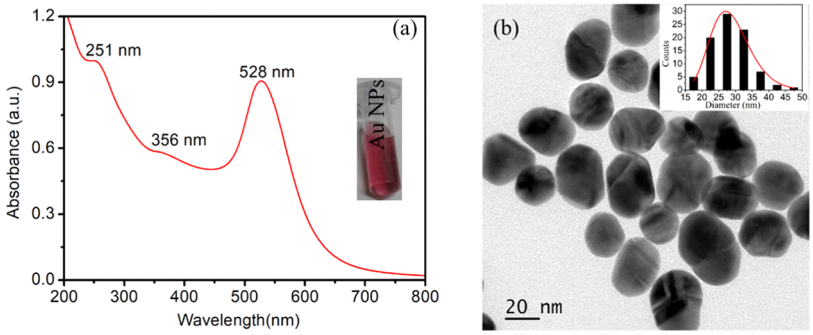

Figure 1. (a) UV−vis absorption spectrum of Au NPs' colloidal dispersion (0.1 mM) and (b) TEM micrograph of the as-synthesized Au NPs. The insets of (a) and (b) show the digital micrographs of the vial containing as-synthesized Au NPs' dispersion and lognormal fitting of the NPs' size distribution curve, respectively.

concentration of the aqueous gold nanocolloidal solution was 0.1 mM at pH ∼ 7 in ambient temperature.

2.3. Characterization Techniques. High-resolution transmission electron microscopy (HRTEM) measurements, energy-dispersive spectroscopy (EDS) images, and selected area electron diffraction (SAED) patterns of the Au NPs were collected using a field emission transmission electron microscope (JEM-2010 TEM, JEOL Ltd., Japan) operated at an accelerating voltage of 200 kV. For the HRTEM study, the sample solutions were incubated for 15 min and then a small drop from each solution was spread onto the carbon-coated copper microgrid (PELCO 300 Mesh Grids, Ted Pella Inc.) and subsequently dried at room temperature (25 °C). The hydrodynamic nanoparticle size and the effective surface ζ potential of the as-synthesized Au NPs were obtained by a Zetasizer (Zetasizer Nano ZS, Malvern Instruments Ltd., U.K.) via the dynamic light scattering (DLS) method at ambient condition. The UV−vis absorption spectra of the samples were obtained in the wavelength range of 200−800 nm by a double-beam UV−vis absorption spectrophotometer (UV-1800, Shimadzu, Japan) after proper baseline correction for the solvent background. The steady-state fluorescence emission spectra of the sample solutions were recorded using a spectrofluorometer (Fluoromax-4C, Horiba Instruments Incorporated, USA) under the following conditions: excitation and emission monochromator slit widths of 2 nm each, excitation wavelength of 530 nm, emission wavelength range of 540−700 nm, and experimental temperature of 25 °C. Fluorescence-grade quartz cuvettes (path length 1.0 cm, Kozima, Japan) were used in all of the absorption and fluorescence emission measurements. CD spectroscopic measurements were carried out using a JASCO J-815 CD spectrometer (JASCO International Co., Ltd., Japan). The surface morphology and roughness measurement of the samples were performed using a commercially available atomic force microscope (AFM) (NaioAFM, Nanosurf, Germany) in tapping mode in a humidity-controlled environment. For AFM analysis, the freshly prepared Au NPs aqueous colloidal dispersion and a mixture of Au NPs/RhB in the presence of D-Cys and L-Cys, respectively, were deposited onto smooth glass substrates. FTIR spectra of the samples were recorded using a FTIR spectrometer (model: Spectrum Two, make: Perkin Elmer Inc.) in attenuated total reflection (ATR) mode at ambient temperature. The pH of the aqueous solutions was measured using a digital pH meter (FiveEasy Plus, Mettler Toledo, Germany).

2.4. Sample Preparation for the Spectrofluorometric Measurements. The Au NPs/RhB mixed solution was prepared by adding 2 mL of freshly prepared Au NPs of concentration 0.1 mM into 2 mL of freshly prepared RhB of concentration 0.1 μM at ambient condition. Thus, the final concentrations of the Au NPs and RhB in the total 4 mL mixed solution were 0.05 mM and 0.05 μM, respectively. The pH of the RhB aqueous solution was 7.0 and remained approximately constant through the whole analysis. Then, a freshly prepared 200 μL aqueous solution of each concentration of D-Cys (concentration range from 1000 μM to 1 nM) was added to the Au NPs/RhB mixed ensemble separately and incubated for 3 min at room temperature (25 °C). Also, the D-Cys aqueous solution was prepared by using ultrapure triple distilled Milli-Q water at pH 7.0. The final concentrations of D-Cys in all of the Au NPs/RhB/D-Cys mixed solutions were in the range 0.0476 nM to 47.6 μM. After the incubation period of 3 min, colorimetric images, the UV−vis absorption, and steady-state fluorescence emission spectra of the Au NPs/RhB/D-Cys complex were recorded immediately. Also, aqueous solutions (fixed concentration of 0.1 mM) of other relevant D- and L-amino acids such as D-arginine (D-Arg), L-arginine (L-Arg), D-histidine (D-His), L-histidine (L-His), D-methionine (D-Met), L-methionine (L-Met), D-proline (D-Pro), L-proline (L-Pro), D-tryptophan (D-Trp), L-tryptophan (L-Trp), D-tyosine (D-Tyr), L-tyosine (L-Tyr), L-cysteine (L-Cys), and other −SH-containing compounds like glutathione (GSH) and homocysteine (Hcys) as well as some different biomolecules such as ascorbic acid (AA), uric acid (UA), and neurotransmitters (Na^+ and K^+) were prepared in the same ambient condition. A 200 μL aqueous solution of each compound was added separately to the Au NPs/RhB mixed solution and incubated for 5 min at ambient condition prior to the spectrofluorometric measurements. The 5 min incubation time used for other analytes except D-Cys was just to confirm whether these other compounds have any effect on the proposed interaction even after a longer time of incubation compared to that of D-Cys.

3. RESULTS AND DISCUSSION

3.1. Characterization of the Au NPs. The UV−vis absorption spectroscopic data were recorded to explore the optical absorption properties of the as-synthesized citrate-stabilized colloidal aqueous dispersion of Au NPs and are shown in Figure 1a. The figure shows a distinct absorption band with its maximum at around 528 nm due to the strong characteristic surface plasmon resonance (SPR) of the Au NPs. Also, there are two weak humps observed at 251 and 356 nm,

https://doi.org/10.1021/acsomega.2c02725
ACS Omega 2022, 7, 29013−29026

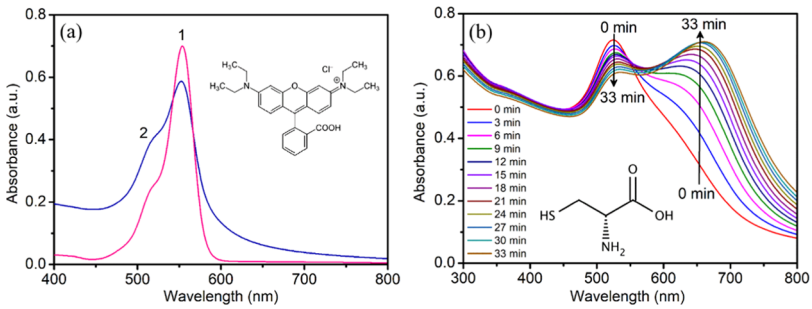

Figure 2. UV−vis absorption spectra of (a) pure RhB aqueous solution (0.1 μM) (curve 1), Au NPs/RhB mixed solution (the concentrations of Au NPs and RhB are 0.05 mM and 0.05 μM in the mixed solution, respectively) (curve 2) and (b) mixed solution of Au NPs and D-Cys (the concentrations of Au NPs and D-Cys are 0.09 mM and 6.25 μM in the mixed solution, respectively) recorded at different intervals of time. The insets of (a) and (b) show the molecular structure of RhB and D-Cys, respectively.

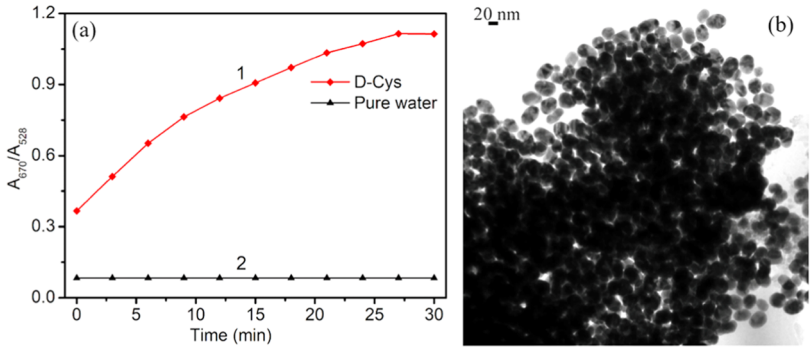

Figure 3. (a) Ratio of the absorbance at 670−528 nm of Au NPs after addition of D-Cys (curve 1) and pure water (200 μL) (curve 2). (b) TEM micrograph of as-synthesized Au NPs after incubation with D-Cys for 15 min at room temperature.

which are mainly attributed to the intraband electronic transitions of gold.[34] The sharp and well-resolved SPR maximum band is originated basically due to both the longitudinal and transverse SPR equivalently, which is an indication of the formation of spherical Au NPs.[35]

The average hydrodynamic diameter of the colloidal Au NPs as obtained from the DLS study was about 48.04 nm (as shown in Figure S1a in the Supporting Information). The surface ζ potential of the Au NPs was found to be −30.1 mV (as shown in Figure S1b in the Supporting Information). The high negative ζ potential reveals the homogeneity and stability of the NPs in the aqueous colloidal dispersion. On the other hand, the TEM micrograph as shown in Figure 1b gives the visual evidence that Au NPs were monodispersed with nearly spherical shape and the average particle diameter was ∼27.5 nm, as is evidenced from the lognormal fitting of the particles' size distribution curve (the inset of Figure 1b obtained from Figure S2a in the Supporting Information). The good crystalline nature of the Au NPs was shown by the SAED pattern (as shown in Figure S2b in the Supporting Information). The rings as shown in SAED were indexed as (311), (222), and (400) and correspond to the electron diffractions originated from the planes of the face-centered cubic (FCC) gold crystal.[36] The interplanar spacing of the as-synthesized FCC Au NPs was 0.11 nm for the (222) plane as calculated from the HRTEM micrograph (as shown in Figure S2c in the Supporting Information). The EDS spectrum (as shown in Figure S2d in the Supporting Information) reveals that the nucleation of Au NPs occurred without any impurities and confirms the presence of a large number of NPs in its aqueous colloidal dispersion.

3.2. UV−Vis Absorption Spectroscopic Study.

The UV−vis absorption spectroscopic measurements were carried out by adding D-Cys and other D- and L-amino acids, neurotransmitters, AA, UA, including other −SH-containing compounds such as Met, HCys, GSH etc., to the mixed solution of Au NPs and RhB (aqueous mixture of Au NPs (0.1 mM) and RhB (0.1 μM) in 1:1 volume ratio). Figure 2a shows the UV−vis absorption spectra of pure RhB (0.1 μM) (curve 1) along with the mixture of RhB and Au NPs in aqueous solution (curve 2). The concentrations of Au NPs and RhB in the mixed solution were 0.05 mM and 0.05 μM, respectively. The inset of Figure 2a shows the molecular structure of the laser dye RhB. The UV−vis absorption spectrum of pure RhB exhibits a strong absorption band at around 554 nm, which is attributed to the $\pi-\pi^*$ transition of the dye monomer unit, and a weak hump is observed at around 520 nm, which is originated from the $n-\pi^*$ transition due to the presence of dimeric units.[24] The UV−vis absorption results of the mixed solution further reveal that the monomeric absorption peak of RhB remains unaltered but with decreased intensity, whereas the dimeric band intensity (520 nm) increases. This variation of the absorption intensity may possibly be due to the closure association of the RhB molecules adsorbed onto the NPs' surface. As RhB is a cationic dye and citrate caped Au NPs have a large negative surface ζ potential, the strong electrostatic interaction between Au NPs and RhB is mainly responsible for the adsorption of the dye molecules on the NPs' surface, resulting in the change in the absorption behavior of the dye molecules in their aqueous mixed solution. The number of dye molecules (N_{dye}) linked with each Au NP is determined using the relation[37] (eq 1)

https://doi.org/10.1021/acsomega.2c02725
ACS Omega 2022, 7, 29013−29026

$$N_{dye} = \frac{n_{Au}}{\{[\text{Au NPs}]/[\text{RhB}]\}} \quad (1)$$

where n_{Au} is the number of gold atoms in each NP. The number of gold atoms per NP (n_{Au}) is calculated by using the expression[37,38] $n_{Au} = (\pi/6)(59\ \text{nm}^{-3})(d_{av})3$, where d_{av} is the mean diameter of the Au NPs. Thus, in this case, an Au NP of average diameter 27.5 nm is composed of 642 138 gold atoms. In the mixed solution of Au NPs (0.1 mM) and RhB (0.1 μM), 642 dye molecules are adsorbed on each Au NP surface.

On the other hand, the UV−vis absorption spectrum of RhB in the presence of D-Cys as shown in Figure S3a in the Supporting Information reveals that there is no appreciable effect of D-Cys on the absorption behavior of RhB in the mixed solution of RhB and D-Cys. The concentration of RhB was kept fixed for all of these mixed solutions, which were prepared using RhB and the Au NPs solution in 1:1 volume ratio. The UV−vis absorption spectra of the Au NPs (concentration of 0.1 mM) recorded at different intervals of time after addition of the aqueous solution of D-Cys (concentration of 0.1 mM) are shown in Figure 2b. The respective concentrations of Au NPs and D-Cys in the mixed solution were 0.09 mM and 6.25 μM. The inset of Figure 2b shows the molecular structure of D-Cys. The additional band of Au NPs observed at around 670 nm is originated due to the strong interaction of D-Cys with the citrate caped Au NPs in the mixed aqueous solution. The absorbance of the main SPR band at around 528 nm gradually decreases and the new band at 670 nm systematically increases with the incubation time for the mixed solution. The absorbance ratio (A_{670}/A_{528}) of the Au NPs colloidal dispersion, as shown in Figure 3a, increases with the incubation time in the presence of D-Cys. This is possibly due to the strong cooperative metal ion-ligand interactions.[39] Because of this interaction, the citrate layer on the nanoparticles' surface may be displaced and the interparticle separations of the NPs are possibly reduced due to the subsequent cross-linking through the amino groups of D-Cys. As a consequence, the increased dipole−dipole interactions and the coupling between neighboring plasmons eventually induced the formation of aggregates or clusters[39,40] of Au NPs. This aggregation is manifested as the emergence of the additional band at around 670 nm in the UV−vis absorption spectra.[41,42] In order to have direct visual evidence for the formation of aggregates or clusters of NPs, TEM analysis was also performed. Figure 3b shows the TEM image of the Au NPs/RhB/D-Cys mixed sample and clearly shows very dense and aggregated domains of the NPs when compared to the TEM image of pure Au NPs as shown in Figure 1b. This aggregation eventually induces enhanced dye−dye intermolecular interaction in the mixed solution of Au NPs and RhB. As a result, the RhB molecules might have altered electric transition dipole moments in the microenvironment of Au NPs.[43]

3.3. Interaction of D-Cys with the Au NPs/RhB Mixed Solution. To understand the interaction of D-Cys with the Au NPs/RhB mixed ensemble in aqueous medium and the related photophysical properties, steady-state fluorescence emission measurements were performed. It is observed from Figure S3c in the Supporting Information that the steady-state fluorescence emission intensity of the peak at around 574 nm of RhB in the Au NPs/RhB mixed aqueous solution (1:1 volume ratio) is almost quenched for an Au NP concentration of 0.05 mM in the mixed solution at ambient condition. It is important to mention that the electrostatic interaction between the dye molecules and the negatively charged citrate layer on the Au NPs or any formation of H bonds does not change the electronic transition dipole moment of the xanthene moiety of the RhB molecules[44] as there is no shift of the emission band (574 nm) of dye molecules after photoexcitation of the Au NPs/RhB mixed ensemble in the absence or presence of D-Cys. Therefore, the effect of direct molecule on nanoparticle interaction may be excluded from the initial fluorescence quenching of RhB molecules in the presence of Au NPs. Additionally, the possibility of dynamic collisional quenching of fluorescence may be less due to the existence of a strong electrostatic interaction between the RhB molecules and negatively charged citrate caped Au NPs in the studied aqueous medium. Interestingly, there is a sufficient spectral overlap between the absorption spectrum of Au NPs and fluorescence emission spectrum of RhB as shown in Figure S3b in the Supporting Information. So, the observed quenching of fluorescence emission (574 nm band) of RhB in the Au NPs/RhB mixed solution is mostly due to the efficient nonradiative energy migration through the resonance energy transfer (RET) process (as shown in Figure S3b,c in the Supporting Information) using the dipole−dipole resonance interaction between the excited RhB dye (donor) molecules and Au NP surface (acceptor), as well as the decrease in the radiative rate constant of individual RhB molecules when they are adsorbed onto the NPs' surface.[21,43] This resonance energy transfer process is a distance-dependent phenomenon and therefore the concentration of the Au NPs (acceptor) plays a significant role in controlling the relative distance between the donor and acceptor sites in the mixed solution. The RET efficiency (E) is calculated using the expression[44,45] (eq 2)

$$E = 1 - \frac{F}{F_0} \quad (2)$$

where F_0 and F are the fluorescence emission intensity of RhB in the absence and presence of Au NPs, respectively. The value of energy transfer efficiency (E) is estimated as 0.9989, considering the fluorescence spectrum of Au NPs/RhB with concentrations of RhB and Au NPs as 0.05 μM and 0.05 mM in the mixed solution, respectively. The value of the binding constant (K_b) to a binding site and the number of binding sites (n) per RhB molecule in the Au NPs/RhB mixed aqueous solution are determined from the fluorescence quenching data of RhB in the presence of Au NPs by using the following eq 3[46]

$$\text{Log}\left\{\frac{F_0 - F)}{F}\right\} = \text{Log}\, K_b + n\ \text{Log}[\text{Q}] \quad (3)$$

where [Q] is the corresponding quencher (Au NPs) concentration. The values of K_b and n are calculated from the intercept and slope of the plot as shown in Figure S3c,d in the Supporting Information and are found to be 2.202×10^3 M^{-1} and 0.376, respectively. The change in Gibbs free energy (ΔG) for the interaction between RhB and Au NPs at room temperature (25 °C) is obtained using the Gibbs−Helmholtz relation[46] $\Delta G = -RT \ln K_b$, where R is the universal gas constant and T is the temperature. The calculated value of ΔG is −19.07 kJ mol^{-1}. The negative ΔG value indicates that the interaction between RhB and Au NPs is spontaneous. Also, the quenching of the fluorescence emission of RhB by Au NPs is further described by the well-known Stern−Volmer equation (eq 4)[47]

https://doi.org/10.1021/acsomega.2c02725
ACS Omega 2022, 7, 29013−29026

Table 1. Binding Constant (K_b), Binding Sites (n), Gibbs Free Energy (ΔG), Stern–Volmer Constant (K_{SV}), and Quenching Rate Constant (K_q) for the Au NPs/RhB Mixed Aqueous Solution[a]

K_b (M^{-1})	n	R^2	ΔG (kJ mol^{-1})	K_{SV} (M^{-1})	R^2	K_q (M^{-1} s^{-1})
2.202×10^3	0.376	0.9924	−19.07	8.174×10^6	0.9924	5.906×10^{15}

[a] R^2 is the corresponding correlation coefficient.

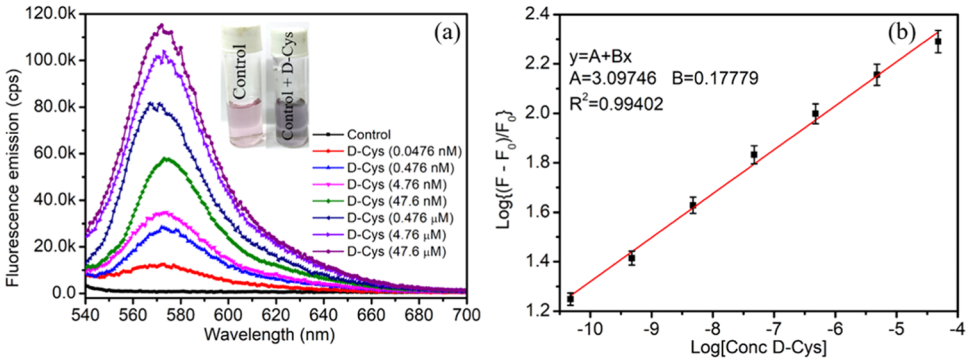

Figure 4. (a) Recovery of fluorescence emission from the Au NPs/RhB mixed solution when added with D-Cys of various concentrations (0.0476 nM to 46.7 μM in the mixed solution). The concentrations of Au NPs and RhB in their mixed solution used here are 0.05 mM and 0.05 μM, respectively. (b) Linear dynamic plot of the fluorescence recovery efficiency of the Au NPs/RhB mixed solution for various concentrations of D-Cys. The inset of (a) shows the digital micrographs of the vial containing the Au NPs/RhB mixed solution before (control) and after incubation for 3 min with D-Cys. The excitation wavelength was 530 nm.

$$\frac{F_0}{F} = 1 + K_{SV}[Q] \quad (4)$$

where K_{SV} is the Stern–Volmer quenching constant. The deviation from linearity of the Stern–Volmer plot at higher quencher concentration implies that the fluorescence quenching of the RhB dye is a mixture of static and dynamic (diffusion) quenching.[48] Considering the slope of the straight-line region of the F_0/F vs [Q] plot (i.e., at lower concentrations of Au NPs) as shown in Figure S3c,e in the Supporting Information, the value of K_{SV} is calculated as 8.174×10^6 M^{-1}. The bimolecular fluorescence quenching rate constant (K_q) and K_{SV} are related by the relation[49] $K_q = K_{SV}/\tau_0$, where τ_0 is the fluorescence emission lifetime of pure RhB (1.384 ns).[21] The value of K_q is calculated as 5.906×10^{15} M^{-1} s^{-1} for this fluorometric titration experiment. The high values of both K_{SV} and K_q substantiate the efficient quenching of RhB (donor) fluorescence by gold nanoparticles in the aqueous medium. All of the above calculated photophysical parameters are summarized in Table 1.

However, interestingly, after addition of D-Cys to the mixed solution of Au NPs and RhB, the original fluorescence emission (574 nm) of dye molecules is recovered from their quenched state as shown in Figure 4a. The concentrations of RhB and Au NPs for the assay experiments were optimized in such a way that there is an almost complete quenching of the fluorescence emission of RhB in the Au NPs/RhB mixed system before addition of the D-Cys solution when excited with light of wavelength 530 nm and recovery of fluorescence signal in the presence of D-Cys at ambient condition. This "turn-off" and "turn-on" mechanism of fluorescence emission due to the presence of D-Cys in the assay medium is schematically shown in Figure 5. For the assay experiments, the concentrations of RhB and Au NPs in their aqueous mixture were fixed at 0.05 μM and 0.05 mM, respectively. These selected concentrations of RhB and Au NPs in their aqueous solution at ambient condition may be considered as an optimized condition for the fluorescence recovery from the mixed ensemble when exposed

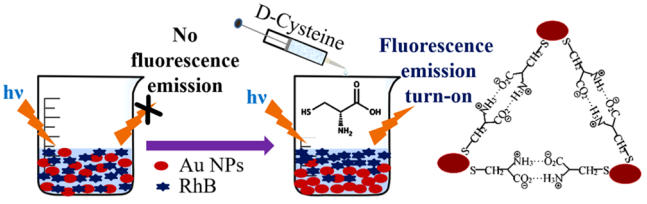

Figure 5. Schematic presentation of the proposed fluorescence "off–on" mechanism and chemical coordination between the D-Cys molecules and citrate caped Au NPs.

to D-Cys in aqueous medium. Here we have studied the recovery of fluorescence emission from the Au NPs/RhB mixed solution in the absence (control) and presence of various concentrations of D-Cys. Also, there is a distinct color change of the mixed final solution from red-wine (control) to bluish-black (after addition of D-Cys) as shown in the inset of Figure 4a. From the fluorescence emission of RhB in the presence of different concentrations of D-Cys (viz. 0.06 nM to 62.5 μM in the mixed solution) as shown in Figure S3f in the Supporting Information, it is further confirmed that there is no significant effect of D-Cys on the fluorescence emission properties of RhB in aqueous solution as the emission spectra of the RhB/D-Cys mixed solution for all concentrations of D-Cys are almost unaltered. Therefore, RhB dye has been considered as a good and efficient fluorescent probe for recognition of the amino acid D-Cys in aqueous medium via a simple spectrofluorometric method in the present work.

It is known that at neutral or under near-physiological pH, citrate caped Au NPs possess three carboxylated ($-COO^-$) groups,[50] whereas the D-Cys molecule has $-SH$, $-COO^-$ groups, and the amino group (NH_3^+) in the same aqueous environment. The citrate layer surrounding the Au NPs in aqueous dispersion gives an overall strong negative surface potential as is already confirmed by the ζ potential study (as shown in Figure S1b in the Supporting Information). It is already reported elsewhere that at neutral pH (7.0) cysteine is

https://doi.org/10.1021/acsomega.2c02725
ACS Omega 2022, 7, 29013−29026

Table 2. Comparisons of the Analytic Methods for the Determination of D-Cysteine

probe/systems	detection principle	range (in μM)	LOD (in nM)	ref
4-fluoro-7-nitrobenzofurazan	SRM-chromatogram	0−300		28
Ag NPs-embedded nanopaper	colorimetric		4880	29
NCS-OTPP[a]	UHPLC-HRMS-chromatograms	0.098−1000	19.20	30
polar ionic elution[b]	chiral UHPLC-MS	0.413−4.13	165.08	31
L-carnitine methyl ester bis	electrokinetic chromatography	10−150	1100	32
Au NPs/RhB mixed system	colorimetric and fluorometric assay	0.001−100	4.2	this work

[a](*R*)-(5-(3-Isothiocyanatopyrrolidin-1-yl)-5-oxopentyl)triphenylphosphonium. [b]MeOH/MeCN/H_2O 49/49/2 v/v/v.

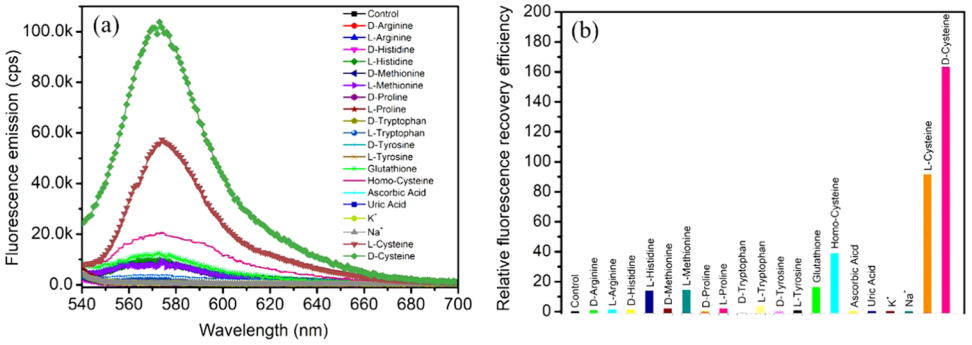

Figure 6. (a) Recovery of fluorescence emission from the Au NPs/RhB mixed solution (concentrations of Au NPs and RhB in their mixed solution are 0.05 mM and 0.05 μM, respectively) in the presence of all of the relevant analytes used in this work. The concentrations of all of the analytes are 47.6 μM in the Au NPs/RhB mixed solution. (b) Relative fluorescence recovery efficiency (at 574 nm) of the Au NPs/RhB mixed solution due to each analyte as calculated from the corresponding emission intensities. Excitation wavelength was 530 nm.

neutral,[51] due to which there will be very less possibility of citrate caped Au NPs having direct interaction with D-Cys through its $-NH_2$ group via electrostatic attraction.[42] However, due to the strong affinity of the −SH moiety of D-Cys towards the Au NPs' surface, they try to encapsulate[41] Au NPs by thiolate−Au bond formation via chemisorption,[39] which eventually displaces the original citrate layer of Au NPs. As a consequence, the RhB molecules that were adsorbed onto the citrate caped nanoparticles' surface by electrostatic interaction[52] now become free in the surrounding environment. This is why the intrinsic fluorescence emission of RhB with peak centered at 574 nm is retrieved after photoexcitation. However, the displacement of the citrate layer of Au NPs should depend upon various factors like the concentration of D-Cys molecules in the assay medium, overall charge distribution, surface potential around the nanoparticle surface, temperature etc. Immediately after the reaction of D-Cys with Au NPs/RhB systems, the presence of amino acid molecules in the encapsulating shell of nanoparticles starts to induce cross-linking (as shown schematically in Figure 5 between the neighboring encapsulated Au NPs) in the mixed solution, resulting in the formation of Au NP aggregates or clusters, which causes a color change of the mixed solution from red-wine to bluish-black[53,54] after the reaction. The aggregation of Au NPs in the presence of D-Cys is already evidenced by the UV−vis absorption (Figure 2b) and TEM study (Figure 3b) as discussed earlier. From the above discussion, it is clear that the fluorescence emission band intensity at 574 nm of the mixed solution of Au NPs and RhB is recovered after addition of D-Cys and this fluorescence recovery is most probably due to the availability of free RhB molecules in the mixed ensemble. Overall, due to the interaction of D-Cys with the Au NPs/RhB system in solution, the relative distance between the dye molecules and Au NPs might have increased, resulting in the decrease of fluorescence quenching via nonradiative energy transfer pathways.

3.4. Sensitivity of the Interaction of the Au NPs/RhB Mixed Ensemble towards D-Cys. In this work, it is important to understand the sensitivity of the interaction of D-Cys with Au NPs/RhB mixed aqueous solution. It is observed that under the optimized experimental condition, the fluorescence emission intensity obtained from the Au NPs/RhB/D-Cys mixed solution increases almost linearly with the increase in concentrations of D-Cys. The relative fluorescence recovery efficiency is defined by $[(F - F_0)/F_0]$ and is given by the following linear equation (eq 5)[52]

$$\mathrm{Log}\left[\frac{(F - F_0)}{F_0}\right] = \mathrm{Log}[\mathrm{C}] + A \quad (5)$$

where C is the concentration of D-Cys and A is an arbitrary constant. The relative fluorescence recovery efficiency and the concentration of D-Cys follow the linear equation $y = 3.09746 + 0.17779[\mathrm{C}]$ with a correlation coefficient (R^2) of 0.99402 as shown in Figure 4b, and the concentration range of 0.004 nM to 47.6 μM in the Au NPs/RhB mixed ensemble. Thus, this method of recovery of fluorescence emission shows very high sensitivity to a broad linear range of concentrations of D-Cys. To compare the sensitivity of Au NPs/RhB towards D-Cys, the limit of detection (LOD) has been determined by the 3σ method[55] using the expression LOD = $(k \times \mathrm{SD})/S$, where S is the slope of the recovered fluorescence emission from the Au NPs/RhB vs concentration of D-Cys (in M) plot (see the Supporting Information for the detailed calculations). The LOD value of D-Cys (as shown in Figure S7a,b,c in the Supporting Information) is found to be 4.2 nM. This LOD value indicates that the proposed Au NPs/RhB mixed ensemble is highly sensitive towards D-Cys for spectrofluorometric measurement. The linear range and LOD of D-Cys

https://doi.org/10.1021/acsomega.2c02725
ACS Omega 2022, 7, 29013−29026

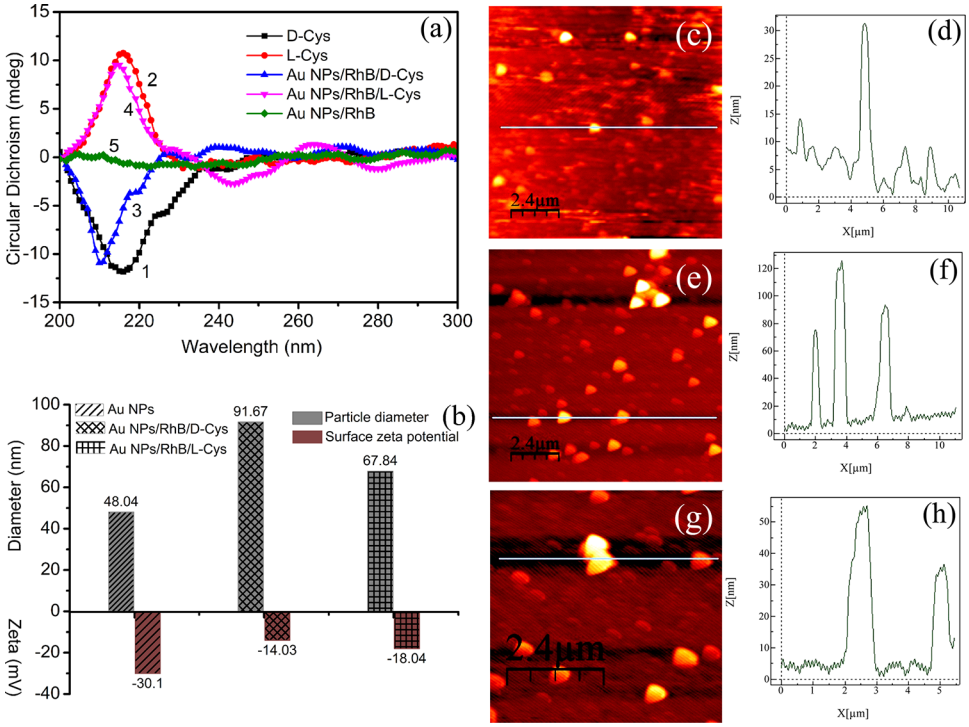

Figure 7. (a) CD spectra of the aqueous solution of pure D-Cys (curve 1, 1 mM), pure L-Cys (curve 2, 1 mM), mixed solution of Au NPs/RhB/D-Cys (curve 3), Au NPs/RhB/L-Cys (curve 4), and Au NPs/RhB (curve 5). (b) Column plot of the hydrodynamic diameter and surface ζ potential of the NPs as obtained from Au NPs/RhB/D-Cys and Au NPs/RhB/L-Cys mixed solutions (c–h). AFM topographic micrographs and surface roughness plot of (c, d) as-synthesized Au NPs, (e, f) Au NPs/RhB/D-Cys mixed system, and (g, h) Au NPs/RhB/L-Cys (g, h) mixed systems deposited on a smooth glass substrate. The RMS surface roughness has been measured along the chosen lines as shown in the figures.

determination as previously reported in the different studies have been compared with the present work and summarized in Table 2.

3.5. Selectivity Study of the Proposed Bio-Nano Interactions. The selectivity of the interaction of the Au NPs/RhB mixed solution towards D-Cys in the presence of other relevant interfering analytes such as AA, UA, neurotransmitters, other D- and L-amino acids including D-Arg, L-Arg, D-His, L-His, D-Met, L-Met, D-Pro, L-Pro, D-Trp, L-Trp, D-Tyr, L-Tyr, L-Cys, −SH-containing compounds like GSH and Hcys etc. is tested under the same optimized experimental conditions of the Au NPs/RhB mixed solution and the corresponding fluorescence emission spectra are illustrated in Figure 6a. The chemical structures of all of the interfering compounds are shown in Figure S4 in the Supporting Information. From Figure 6a it is observed that the fluorescence emission intensities of the Au NPs/RhB mixed solution in the presence of D-Cys and L-Cys are significantly high compared to those for other interfering compounds, although the concentrations of all of the analytes were the same in these spectrofluorometric measurements. However, when the Au NPs/RhB mixed solution is added with D-Cys, the final solution turns red-wine to bluish-black in color, which is different when mixed with L-Cys solution separately, as shown in Figure S5 in the Supporting Information. The relative fluorescence recovery efficiency $[(F - F_0)/F_0]$ as shown in Figure 6b becomes remarkably high for D-Cys compared to that for all other relevant interfering species or elements. From the above observations it is clear that the interaction of the Au NPs/RhB mixed ensembles with D-Cys in aqueous medium is selective due to the high fluorescence recovery as well as distinct color change of the Au NPs/RhB mixed solution when compared to the interactions with L-Cys and all other D- and L-amino acids, physiologically relevant interfering elements etc. as studied in this experiment. It is important to mention that the difference between fluorescence recovery efficiencies for D-Cys and L-Cys might be attributed to the different chiralities in the molecular structure of these amino acids, as is evidenced from the CD spectra shown in Figure 7a. The high selectivity of the interaction of the Au NPs/RhB mixed solution with D-Cys may be attributed to the change in structural configuration of the amino acid D-Cys, which is manifested as the observed change in the peak position of the CD spectrum. This is because any change in the configuration of the functional group (−SH) while interacting with the Au NPs/RhB mixed ensemble in aqueous medium possibly disrupts the chiral properties in the structure of D-Cys. As a result, there is a blue shift of the peak position at 210 nm in the CD spectrum as shown in Figure 7a. On the other hand, when L-Cys is added to the Au NPs/RhB mixed solution, the peak position observed at 216 nm in the CD spectrum is not altered except for a slight reduction of intensity. These observations clearly indicate that the chiral properties of L-Cys were possibly less affected while interacting with the Au NPs/RhB mixed ensemble compared to those of D-Cys. From the DLS study, as shown in Figures 7b, S8a, and S9a, it is observed that the particle size of Au NPs increases in the presence of both D- and L-Cys. However, for D-Cys, the increase in hydrodynamic particle diameter is higher (91.67 nm) compared to that of L-Cys (67.84 nm). This observation implies the possibility of a high degree of aggregation of Au NPs while interacting with D-Cys when compared to that due to L-Cys. As mentioned earlier, amino acids basically displace the citrate layer of the Au NPs during interaction and induce interparticle cross-linking, which favors

https://doi.org/10.1021/acsomega.2c02725
ACS Omega 2022, 7, 29013−29026

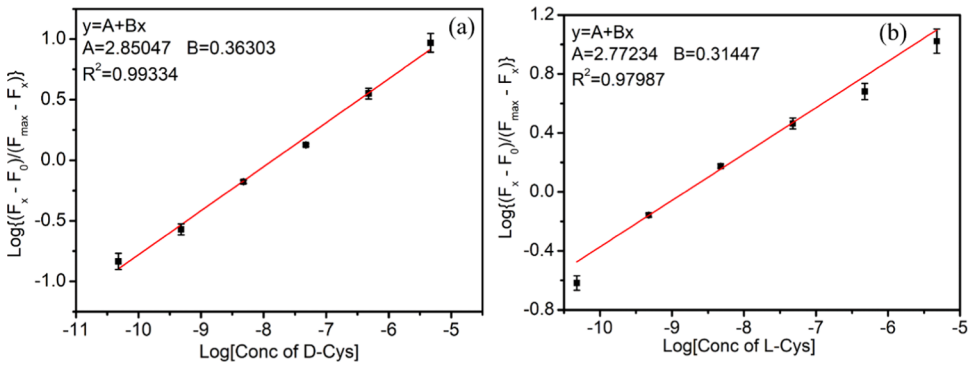

Figure 8. Plot of (a) Log{$(F_x - F_0)/(F_{max} - F_x)$} vs Log[concentration of D-Cys] and (b) Log{$(F_x - F_0)/(F_{max} - F_x)$} vs Log[concentration of L-Cys] to determine the binding constants of the Au NPs/RhB system with D-Cys and L-Cys, respectively.

rapid aggregation of Au NPs. However, the rate or extent of interparticle cross-linking is possibly higher for D-Cys than for L-Cys. Additionally, the less negative ζ potential (Figures 7b, S8b, and S9b) of the Au NPs/RhB mixed solution containing D-Cys (−14.03 mV) compared to that with L-Cys (−18.04 mV) confirms the higher aggregation of NPs in the case of D-Cys.[56] To have a better understanding and direct visual evidence of the formation of aggregates or clusters, AFM topographical imaging is performed in a tapping mode. Figure 7c–h shows the AFM topographical image and surface roughness plot of the drop-casted film deposited onto smooth glass substrates from the Au NPs/RhB mixed solution in the presence of D-Cys and L-Cys, respectively. For all of these measurements, Au NPs/RhB mixed solutions were prepared in 1:1 volume ratio and their concentrations in the mixed solution were 0.05 mM and 0.05 μM, respectively. These images show that D-Cys facilitates a higher extent of aggregation or formation of clusters of Au NPs in the mixed solution. The root-mean-square (RMS) surface roughness of the Au NPs/RhB film is estimated as 4.4 nm, whereas for L-Cys and D-Cys it becomes 7.25 and 18.92 nm, respectively. That is, the surface roughness of the film having D-Cys is much higher compared to that of L-Cys. Our AFM analysis revels that D-Cys induces a much greater degree of nanoparticle aggregation. Also, the hydrogen bond between the neighboring D-Cys molecules in the aqueous solution is highly affected by the steric hindrance due to the presence of Au NPs. The high extent of aggregation of NPs in the aqueous mixture of Au NPs/RhB facilitated higher fluorescence recovery from the quenched state due to the release of more number of RhB dye molecules from the Au surface.

Interestingly, our proposed Au NPs/RhB mixed platform does not show any significant or appreciable fluorescence recovery by other aminothiols such as Hcys and GSH in the same aqueous medium as studied in this work. In case of Hcys and GSH, we observe a slight recovery of fluorescence emission from the Au NPs/RhB matrix in aqueous medium. Although Hcys is a homologue of the amino acid Cys, it differs with an additional methylene bridge in its molecular structure. It is also known that[57] nearly at physiological pH, Hcys contains one amino group ($-NH_3^+$), one $-COO^-$ group, and one −SH group in aqueous medium, whereas citrate caped Au NPs possess three $-COO^-$ groups in the same aqueous medium. Therefore, the direct electrostatic binding between Hcys and Au NPs is minimal. Due to the presence of the −SH group in Hcys, there will be still some interaction via thiolate–Au bond formation, but the rate of displacing the citrate layer on which the cationic RhB molecules are bound might be limited due to the difference in the orientation of the amino acid groups or in the interfacial free energies when compared to D-Cys or L-Cys in the studied aqueous environment.[41] As a consequence, the fluorescence emission recovery from the Au NPs/RhB mixed ensemble is less compared to D-Cys and L-Cys. On the other hand, GSH has two −COOH groups associated with glutamic acid and glycine residues and three amino groups ($-NH_3^+$) in three amino acids, and one sulfur atom present in the Cys residue. It is expected that at intermediate or higher pH the disassociation of −COOH groups may hinder[58] the binding of GSH with Au nanocolloids via the α amine group. This results in a very little cross-linking between the −SH group and Au colloids. As we have studied the binding interactions at neutral pH (7.0), less interaction between Au and GSH results in lower fluorescence recovery in the Au NPs/RhB aqueous medium. Additionally, the GSH molecule is relatively bulky in size compared to cysteine or Hcys, and therefore, the interfacial reactivity may be less probable due to energetic consideration. However, literature revels that the amino acid Trp can selectively bind with Au NPs.[59] In the present work, we did not find any significant fluorescence recovery from the Au NPs/RhB mixed solution in the presence of D- and L-Trp. This is possibly due to the formation of the nonfluorescent Trp–RhB complex.[60]

The binding constant, sometimes referred to as the association constant (K_a), of the Au NPs/RhB system with D-Cys and L-Cys in the aqueous medium has been determined using the Benesi–Hildebrand equation (eq 6)[61,62]

$$\frac{1}{(F_x - F_0)} = \frac{1}{(F_{max} - F_0)} + \frac{1}{K_a[M](F_{max} - F_0)} \quad (6)$$

where F_o, F_x, and F_{max} are the fluorescence emission intensities obtained from the mixture of Au NPs/RhB in the absence of D-Cys (or L-Cys), with an intermediate concentration of D-Cys (or L-Cys) and the concentration of D-Cys (or L-Cys) at saturation level, and [M] is the concentration of D-Cys (or L-Cys). The magnitude of the binding constant (K_a) gives an indication about the strength of interaction between the guest and host for their complexation in a medium and is related to the change in Gibbs free energy[46] ($\Delta G = -RT \ln K_a$) for the process. The values of K_a have been obtained from the intercept of the plot of Log{$(F_x - F_0)/(F_{max} - F_x)$} vs Log[M] as shown in Figure 8 for both D-Cys and L-Cys, and are summarized in Table 3. These values confirm that both D-Cys and L-Cys can bind to the Au NPs/RhB system in aqueous solution. But, in the case of D-Cys, this interaction is stronger

https://doi.org/10.1021/acsomega.2c02725
ACS Omega 2022, 7, 29013−29026

Table 3. Binding Constant (K_a) and Gibbs Free Energy (ΔG) for D-Cys and L-Cys with the Au NPs/RhB Mixed Systems in Aqueous Solution[a]

chiral amino acids	K_a (M^{-1})	R^2	ΔG (kJ mol^{-1})
D-Cys	708.712	0.9933	−16.261
L-Cys	592.025	0.9798	−15.816

[a] R^2 is the corresponding correlation coefficient.

than that for L-Cys. Therefore, due to the strong binding interaction between D-Cys and citrate caped Au NPs in aqueous medium, the fluorescence recovery efficiency is much higher compared to L-Cys. The values of the Gibbs free energy ΔG and binding constant K_a for Au NPs/RhB/D-Cys and Au NPs/RhB/L-Cys complexes have been calculated from the steady-state fluorescence emission spectra and are summarized in Table 3. The negative ΔG indicates that the interactions of both D-Cys and L-Cys with the Au NPs/RhB system are spontaneous. However, the higher negative value of ΔG reveals the faster rate of interaction in the case of D-Cys with the assay medium compared to that for L-Cys.

For further investigation on the selectivity and interaction mechanism of Au NPs/RhB with D- and L-Cys, FTIR spectroscopic measurements in ATR mode were performed and are shown in Figure 9. The FTIR spectra of pure D-Cys and L-Cys (curve 1 in (a) and (b), respectively) are very similar and show IR bands with peaks centered at 3166, 1582, and 1390 cm^{-1}, which are attributed to the stretching of $-NH_3^+$ and the asymmetric and symmetric stretching of the $-COO^-$ functional groups of Cys molecules, respectively. In addition, Cys molecules have a weak IR vibrational band near 2550 cm^{-1}, which is originated due to the characteristic stretching vibration of the S−H bond (thiol group). Other vibrational bands are observed at 2968 cm^{-1} (CH_2 stretching, asymmetric), 2078 cm^{-1} (NH_3 bending, asymmetric), 1522 cm^{-1} (N−H bending), 1340 cm^{-1} (NH_3 bending, symmetric), 1294 cm^{-1} (CH_2 wagging), 1195 cm^{-1} (CH_2 twisting), 1130 cm^{-1} (SO_2 stretching), 1062 cm^{-1} (NH_3 rocking), 941 cm^{-1} (S−H bending), 866 cm^{-1} (N−O stretching), 635 cm^{-1} (COOH bending), 536 cm^{-1} (COOH rocking) etc. These results are consistent with the FTIR spectra of amino acids reported elsewhere.[63−65] Interestingly, for the Au NPs/RhB/D-Cys system, the IR bands corresponding to the stretching of $-NH_3^+$ and $-COO^-$ groups of D-Cys are almost absent, possibly due to their cross-linking with other cysteine molecules attached to the neighboring Au NPs. However, for the Au NPs/RhB/L-Cys system, the bands of these stretching vibrations are also abruptly reduced compared to pure L-Cys but the peaks are still visible. These observations may reveal that the interparticle cross-linking is much stronger in the case of D-Cys in the assay medium, resulting in a rapid and greater extent of nanoparticle aggregations, which is reflected in the different color change of the final solution. This may also be due to the change in their dipole moments when binding with a high electron density of the metal surface. But the most significant observation is that the S−H stretching vibration band (2550 cm^{-1}) totally disappears for D-Cys after interacting with the Au NPs/RhB mixed system in aqueous medium (Figure 9a curve 3). This indicates that S−H bonds are cleaved in the presence of the metal NPs, which further indicates the strong binding interaction of D-Cys with Au NPs. On the other hand, the S−H stretching vibration band is not totally absent for L-Cys when interacted with the Au NPs/RhB system but it appears as a weak band near 2550 cm^{-1} as shown in Figure 9b (curve 3). Therefore, it is clear that the interaction of D-Cys with the Au NPs/RhB mixed system is stronger compared to that of L-Cys in the studied aqueous medium. Additionally, the FTIR spectra of the Au NPs/RhB mixed system (curve 2 in Figure 9a,b, respectively) confirm that there is no such significant effect of RhB molecules on the interaction of D-Cys or L-Cys molecules with Au NPs in the assay medium.

3.6. Real Biosample Analysis. The proposed nano-bio interaction is also studied in the presence of normal human urine. The normal urine sample was collected from a healthy laboratory volunteer (male researcher) having no renal complications. In this investigation with the normal urine sample, we maintained the same optimized concentrations of RhB and Au NPs in their mixed solution as discussed earlier, and took extra precautions to avoid any direct contact or any type of contamination with the urine sample. D-Cys may present in both urine and blood plasma. It is already known that diseases like cystinuria leading to the formation of kidney and renal system stone occur due to the free presence of Cys in the urine.[66,67] The fluorescence emission spectra of the mixed solution of Au NPs/RhB (control) in the presence of normal urine (200 μL), mixture of normal urine (200 μL) and D-Cys (0.1 mM, 200 μL), and mixture of normal urine (200 μL) and all other analytes (0.1 mM) used in the present work except D-Cys are shown in Figure S10 in the Supporting Information. The concentrations of D-Cys and all other analytes in the final assay medium containing urine were 2.38 μM, respectively. The corresponding fluorescence recovery efficiency is shown in Figure 10. From this figure it is clear that, the normal urine shows fluorescence recovery efficiency of 42% but mixture of normal urine and D-Cys shows fluorescence recovery efficiency of 73%. Therefore, the usual presence of Cys in the normal

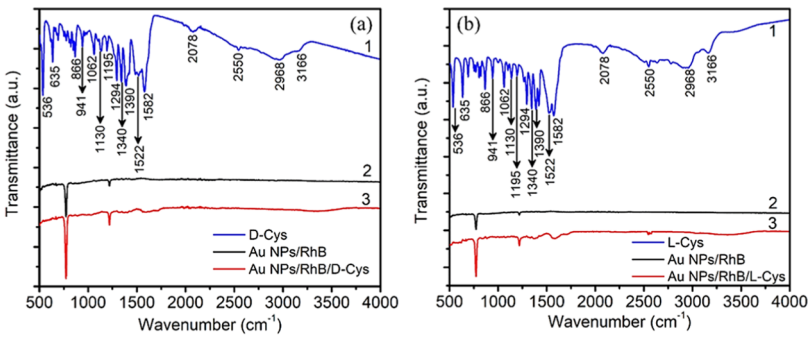

Figure 9. ATR-FTIR spectra of (a) D-Cys (b) and L-Cys in the absence and presence of Au NPs/RhB, respectively.

https://doi.org/10.1021/acsomega.2c02725
ACS Omega 2022, 7, 29013−29026

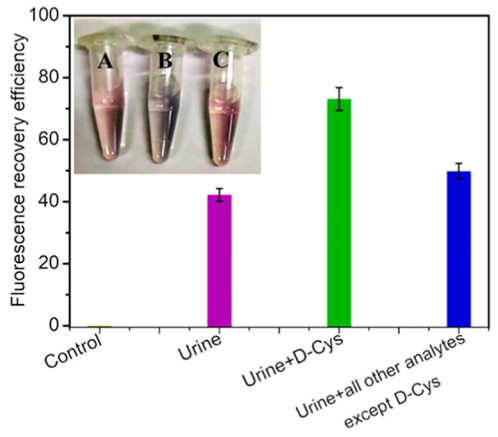

Figure 10. Plot of the fluorescence recovery efficiencies for the Au NPs/RhB mixed solution in the presence of normal human urine and all other analytes relevant to the present work. The inset shows the digital photograph of vials containing the Au NPs/RhB mixed solution with (A) urine, (B) mixture of urine and D-Cys, and (C) mixed solution of urine and all other analytes except D-Cys. The photograph and fluorescence emission spectra are taken after 3 min of incubation for all of these mixed solutions.

urine gives the initial fluorescence recovery from Au NPs/RhB system. It is also observed that when all other D and L-amino acids along with the other relevant interfering compounds as considered are mixed with the proposed assay matrix, the fluorescence recovery efficiency is slightly higher than that due to pure normal urine. This may be due to the presence of L-Cys as was added with all other interfering compounds. Additionally, there is also a distinct color change (from red-wine to bluish-black) of the assay solution after addition of D-Cys compared to all other analytes including L-Cys as shown in the inset of Figure 10. This study confirms the proposed nano-bio interaction is manifested as the selective binding of D-Cys with Au NPs/RhB in in human urine as well. Therefore, the proposed Au NPs/RhB system in aqueous medium under the appropriate and optimized condition may be used as an efficient platform for rapid detection of D-Cys in human urine in a ratio-metric approach to diagnose various renal complications.

4. CONCLUSIONS

In conclusion, we demonstrate a simple fluorometric method to explore the comparative and selective interaction of the amino acid D-Cys among various other D- and L-amino acids, neurotransmitters, relevant biological compounds etc., with citrate caped gold nanoparticles (27.5 nm) in the presence of the fluorescent dye RhB. Au NPs are found to almost fully quench the fluorescence emission of RhB dye in the optimized concentrations of both Au NPs and RhB via a nonradiative energy transfer pathway from the excited RhB molecules to Au NPs in aqueous solution at neutral pH. This quenched fluorescence is selectively recovered with high efficiency after addition of D-Cys to the Au NPs/RhB mixed solution and there was a distinct color change of the assay medium after reaction with D-Cys when compared to the effect of other interfering compounds studied in this work. The degree of aggregation of Au NPs is greater due to the interaction with D-Cys compared to L-Cys due to strong thiolate−Au bond formation via chemisorption and possibly greater interparticle cross-linking compared to that due to L-Cys and in aqueous solution. The higher value of binding constant and higher negative value of Gibbs free energy for D-Cys interacting with the Au NPs/RhB mixed system compared to those for L-Cys as estimated from the fluorescence recovery results confirm the stronger interaction of D-Cys with the nanoparticle system in the studied aqueous medium. The difference in aggregations of D-Cys and L-Cys while interacting with Au NPs/RhB mixed systems in solution is correlated with the ζ potential results and chiral properties of the amino acids, as evidenced by the ζ potential study and CD spectroscopic characterization, respectively. The ATR-FTIR study further distinguishes the difference of interactions of both D-Cys and L-Cys with the assay matrix through the change in vibrational signatures of the S−H bond as well as other relevant functional groups and is consistent with the observations by the other analytical methods used in this present work. The interaction of D-Cys with the proposed nanoparticle-based platform is highly sensitive and lies in the broad linear range of concentration of 1 nM to 100 μM. The LOD for D-Cys is found to be 4.2 nM, which is lower compared to many available detection methods cited in the literature. The normal human urine sample when mixed with the assay matrix (Au NPs/RhB) and D-Cys exhibits a higher fluorescence recovery and distinct color change (red-wine to bluish-black) of the assay medium after reaction compared to that for L-Cys or all other interfering compounds as studied. Therefore, the proposed bio-nano interaction may be realized as an efficient approach for the selective recognition of the amino acid D-Cys in the aqueous environment.

■ ASSOCIATED CONTENT

Supporting Information

The Supporting Information is available free of charge at https://pubs.acs.org/doi/10.1021/acsomega.2c02725.

DLS and ζ potential spectra of Au NPs; TEM micrograph of Au NPs for lognormal fitting of particle size distribution plot; SAED pattern for crystalline nature of Au NPs; HRTEM micrograph to calculate lattice spacing; EDS spectrum for the identification of Au peaks; UV−vis spectra of RhB and RhB/D-Cys; spectral overlap between UV−vis absorption spectrum of Au NPs and fluorescence emission spectrum of RhB for RET; fluorescence emission quenching of pure RhB in presence of different concentration of Au NPs; Log$\{(F_0 - F)/F\}$ vs Log[Conc of Au NPs] plot to obtained binding constant (K_b) and number of binding sites (n) of Au NPS/RhB mixed ensembles; Stern−Volmer plot to determine the Stern−Volmer constant (K_{SV}) of RhB in Au NPs/RhB complex; fluorescence emission spectra of RhB and mixture of RhB/D-Cys; chemical structure of amino acids and biomolecules for selectivity study; colorimetric response from mixed solution of Au NPs/RhB, Au NPs/RhB/D-Cys and Au NPs/RhB/L-Cys; recovery of fluorescence emission from Au NPs/RhB mixed solution in presence of different concentrations of L-Cys; determination of limit of detection (LOD) of Au NPs/RhB towards D-Cys by 3σ method; DLS and ζ potential spectra Au NPs/RhB/D-Cys and Au NPs/RhB/L-Cys; real bio-sample analysis—fluorescence emission spectra of Au NPs/RhB in presence of normal human urine, mixture of urine and D-Cys, mixture of urine and all other relevant analytes except D-Cys (PDF)

https://doi.org/10.1021/acsomega.2c02725
ACS Omega 2022, 7, 29013−29026

AUTHOR INFORMATION

Corresponding Author

Pabitra Kumar Paul − *Department of Physics, Jadavpur University, Kolkata 700032, India;* orcid.org/0000-0002-3490-525X; Phone: +91-9477631142; Email: pabitra_tu@yahoo.co.in, pabitrak.pal@jadavpuruniversity.in; Fax: 91-33-24138917

Authors

Pradip Maiti − *Department of Physics, Jadavpur University, Kolkata 700032, India;* orcid.org/0000-0001-6879-591X

Ujjal Saren − *Department of Physics, Jadavpur University, Kolkata 700032, India;* orcid.org/0000-0003-2949-9987

Utsav Chakraborty − *Department of Physics, Jadavpur University, Kolkata 700032, India;* orcid.org/0000-0003-1528-0335

Tanmoy Singha − *Department of Physics, Jadavpur University, Kolkata 700032, India;* orcid.org/0000-0002-4683-6204

Sharmistha Paul − *West Bengal State Council of Science and Technology, Department of Science and Technology and Biotechnology, Kolkata 700064, India*

Complete contact information is available at: https://pubs.acs.org/10.1021/acsomega.2c02725

Notes

The authors declare no competing financial interest.

ACKNOWLEDGMENTS

P.M. wishes to thank Jadavpur University and Rashtriya Uchchatar Shiksha Abhiyan (RUSA) 2.0 (ref no. R-11/604/19) for providing excellent infrastructural and financial support to perform the experimental studies. P.M., S.P., and P.K.P. are also grateful to the West Bengal State Council of Science and Technology (WBSCST), Govt. of West Bengal for financial assistance (ref no. 493/WBSCST/F/0545/15(Pt-I)) to perform this work. P.K.P. is also thankful to SERB DST, Govt. of India for finanical assistance through the project (ref no. SB/EMEQ-142/2014). The authors are grateful to CSS of the Indian Association for the Cultivation of Science, Kolkata for providing the HRTEM and CD measurements facility used in this work. The authors are also grateful to Prof. Partha Roy of the Department of Chemistry at Jadavpur University for providing access to the ATR-FTIR measurements in this study.

REFERENCES

(1) Widlak, W. *Molecular Biology Not Only for Bioinformaticians*; Springer, 1998.

(2) Kessel, A.; Ben-Tal, N. *Introduction to Proteins Structure, Function, and Motion*, 2nd ed.; CRC Press, 2018.

(3) Kimura, R.; Tsujimura, H.; Tsuchiya, M.; Soga, S.; Ota, N.; Tanaka, A.; Kim, H. Development of a cognitive function marker based on D-amino acid proportions using new chiral tandem LC-MS/MS systems. *Sci. Rep.* **2020**, *10*, No. 804.

(4) Carenzi, G.; Sacchi, S.; Abbondi, M.; Pollegioni, L. Direct chromatographic methods for enantioresolution of amino acids: recent developments. *Amino Acids* **2020**, *52*, 849−862.

(5) Liu, J.; Fu, B.; Zhang, Z. Ionic Current Rectification Triggered PhotoelectrochemicalChiral Sensing Platform for Recognition of Amino Acid Enantiomers on Self-StandingNanochannel Array. *Anal. Chem.* **2020**, *92*, 8670−8674.

(6) Karakawa, S.; Shimbo, K.; Yamada, N.; Mizukoshi, T.; Miyano, H.; Mita, M.; Lindner, W.; Hamase, K. Simultaneous analysis of d-alanine, d-aspartic acid, and d-serine using chiral high-performance liquid chromatography-tandem mass spectrometry and its application to the rat plasma and tissues. *J. Pharm. Biomed. Anal.* **2015**, *115*, 123−129.

(7) Liu, D.; Lv, Y.; Chen, M.; Cheng, D.; Song, Z.; Yuan, L.; Zhang, X. A long wavelength emission two-photon fluorescent probe for highly selective detection of cysteine in living cells and an inflamed mouse model. *J. Mater. Chem. B* **2019**, *7*, 3970−3975.

(8) Winther, J. R.; Thorpe, C. Quantification of thiols and disulfides. *Biochim. Biophys. Acta, Gen. Subj.* **2014**, *1840*, 838−846.

(9) Chen, X.; Hu, Y.; Cao, Z.; Liu, Q.; Cheng, Y. Cerebrospinal Fluid Inflammatory Cytokine Aberrations in Alzheimer's Disease, Parkinson's Disease and Amyotrophic Lateral Sclerosis: A Systematic Review and Meta-Analysis. *Front. Immunol.* **2018**, *9*, No. 2122.

(10) Kjældgaard, A.-L.; Pilely, K.; Olsen, K. S.; Pedersen, S. W.; Lauritsen, A. O.; Moller, K.; Garred, P. Amyotrophic lateral sclerosis: The complement and inflammatory hypothesis. *Mol. Immunol.* **2018**, *102*, 14−25.

(11) Pichette, J.; Gagnon, J. Implications of Hydrogen Sulfide in Glucose Regulation: How H_2S Can Alter Glucose Homeostasis through Metabolic Hormones. *Oxid. Med. Cell. Longevity* **2016**, *2016*, No. 3285074.

(12) Tong, Z.; Ni, L.; Ling, J. Antibacterial peptide nisin: A potential role in the inhibition of oral pathogenic bacteria. *Peptides* **2014**, *60*, 32−40.

(13) Zhang, M.; Ye, B. C. Colorimetric Chiral Recognition of Enantiomers Using the Nucleotide-Capped Silver Nanoparticles. *Anal. Chem.* **2011**, *83*, 1504−1509.

(14) Rodríguez-Zamora, P.; Angeles, B. S.; Buendía, F.; Silis, C. C.; Fabila, J.; Díaz, J. B.; Díaz, L. M. F.; Borbón, L. O. P.; Díaz, G.; Garzón, I. L. Revisiting the conformational adsorption of L- and D-cysteine on Au nanoparticles by Raman spectroscopy. *J. Raman Spectrosc.* **2020**, *51*, 243−255.

(15) Klein, J. Probing the interactions of proteins and nanoparticles. *Proc. Natl. Acad. Sci. U.S.A.* **2007**, *104*, 2029−2030.

(16) Lei, J.; Ju, H. Signal amplification using functional nanomaterials for biosensing. *Chem. Soc. Rev.* **2012**, *41*, 2122−2134.

(17) Zhu, J.; Shen, J.; Hu, B.; Yang, L.; Jiang, C. Chromaticity Evolutionary Detection of Food Contaminant Semicarbazide through an Upconversion Luminescence-Based Nanosensor. *Anal. Chem.* **2022**, *94*, 1126−1134.

(18) Goas, M. L.; Saber, J.; Bolívar, S. G.; Rabanel, J. M.; Awogni, J. M.; Boffito, D. C.; Banquy, X. (In)stability of ligands at the surface of inorganic nanoparticles: A forgotten question in nanomedicine? *Nano Today* **2022**, *45*, No. 101516.

(19) Li, J.; Liu, J.; Chen, C. Remote Control and Modulation of Cellular Events by Plasmonic Gold Nanoparticles: Implications and Opportunities for Biomedical Applications. *ACS Nano* **2017**, *11*, 2403−2409.

(20) Maduraiveeran, G.; Sasidharan, M.; Ganesan, V. Electrochemical sensor and biosensor platforms based on advanced nanomaterials for biological and biomedical applications. *Biosens. Bioelectron.* **2018**, *103*, 113−129.

(21) Maiti, P.; Singha, T.; Chakraborty, U.; Roy, S. D.; Karmakar, P.; Dey, B.; Hussain, S. A.; Paul, S.; Paul, P. K. Selective and sensitive detection of L-Cysteine via fluorometric assay using gold nanoparticles and Rhodamine B in aqueous medium. *Mater. Chem. Phys.* **2019**, *234*, 158−167.

(22) Dizman, H. M.; Kazancioglu, E. O.; Shigemune, T.; Takahara, S.; Arsu, N. High sensitivity colorimetric determination of L-cysteine using gold nanoparticles functionalized graphene oxide prepared by photochemical reduction method. *Spectrochim. Acta, Part A* **2022**, *264*, No. 120294.

(23) Shemetov, A. A.; Nabiev, I.; Sukhanova, A. Molecular Interaction of Proteins and Peptides with Nanoparticles. *ACS Nano* **2012**, *6*, 4585−4602.

(24) Bigdeli, A.; Ghasemi, F.; Moayed, S. A.; Shahrajabian, M.; Kashani, N. F.; Jafarinejad, S.; Nejad, M. A. F.; Nezhad, M. R. H. Ratiometric fluorescent nanoprobes for visual detection: Design

https://doi.org/10.1021/acsomega.2c02725
ACS Omega 2022, 7, 29013−29026

principles and recent advances - A review. *Anal. Chim. Acta* **2019**, *1079*, 30−58.
(25) Yang, X. F.; Guo, X. Q.; Zhao, Y. B. Development of a novel rhodamine-type fluorescent probe to determine peroxynitrite. *Talanta* **2002**, *57*, 883.
(26) Han, S.; Yang, L.; Wen, Z.; Chu, S.; Wang, M.; Wang, Z.; Jiang, C. A dual-response ratiometric fluorescent sensor by europium-doped CdTe quantum dots for visual and colorimetric detection of tetracycline. *J. Hazard. Mater.* **2020**, *398*, No. 122894.
(27) Yang, F.; Lin, D.; Pan, L.; Zhu, J.; Shen, J.; Yang, L.; Jiang, C. Portable Smartphone Platform Based on a Single Dual-Emissive Ratiometric Fluorescent Probe for Visual Detection of Isopropanol in Exhaled Breath. *Anal. Chem.* **2021**, *93*, 14506−14513.
(28) Ferré, S.; Ruiz, V. G.; Zangari, J.; Girel, S.; Martinou, J. C.; Sardella, R.; Rudaz, S. Separation and determination of cysteine enantiomers in plasma after derivatization with 4-fluoro-7-nitro-benzofurazan. *J. Pharm. Biomed. Anal.* **2022**, *209*, No. 114539.
(29) Zor, E. Silver nanoparticles-embedded nanopaper as a colorimetric chiral sensing platform. *Talanta* **2018**, *184*, 149−155.
(30) Ma, Q.; Qi, C.; Li, X. L.; Shi, Q.; Xu, C. Y.; Jin, T.; Min, J. Z. Simultaneous Determination of DL-cysteine, DL-homocysteine, and glutathione in saliva and urine by UHPLC-Q-Orbitrap HRMS: Application to studies of oxidative stress. *J. Pharm. Biomed. Anal.* **2021**, *196*, No. 113939.
(31) Pucciarini, L.; González-Ruiz, V.; Zangari, J.; Martinou, J. C.; Natalini, B.; Sardella, R.; Rudaz, S. Development and validation of a chiral UHPLC-MS method for the analysis of cysteine enantiomers in biological samples. *J. Pharm. Biomed. Anal.* **2020**, *177*, No. 112841.
(32) Greño, M.; Marina, M. L.; Puyana, M. C. Use of single and dual systems of γ- cyclodextrin or γ -cyclodextrin/L-Carnitine derived ionic liquid for the enantiomeric determination of cysteine by electrokinetic chromatography. A comparative study. *Microchem. J.* **2021**, *169*, No. 106596.
(33) Frens, G. Controlled Nucleation for the Regulation of the Particle Size in Monodisperse Gold Suspensions. *Nat. Phys. Sci.* **1973**, *241*, 20.
(34) Dutta Roy, S.; Ghosh, M.; Chowdhury, J. Adsorptive parameters and influence of hot geometries on the SER(R) S spectra of methylene blue molecules adsorbed on gold nanocolloidal particles. *J. Raman Spectrosc.* **2015**, *46*, 451−461.
(35) Jones, M. R.; Osberg, K. D.; Macfarlane, R. J.; Langille, M. R.; Mirkin, C. A. Templated Techniques for the Synthesis and Assembly of Plasmonic Nanostructures. *Chem. Rev.* **2011**, *111*, 3736−3827.
(36) Zhang, J.; Zhao, B.; Meng, L.; Wu, H.; Wang, X.; Li, C. Controlled synthesis of gold nanospheres and single crystals in hydrogel. *J. Nanopart. Res.* **2007**, *9*, 1167−1171.
(37) Chandrasekharan, N.; Kamat, P. V.; Hu, J.; Jones, G., II Dye-Capped Gold Nanoclusters: Photoinduced Morphological Changes in Gold/Rhodamine 6G Nanoassemblies. *J. Phys. Chem. B* **2000**, *104*, 11103−11109.
(38) Acres, R. G.; Feyer, V.; Tsud, N.; Carlino, E.; Prince, K. C. Mechanisms of Aggregation of Cysteine Functionalized Gold Nanoparticles. *J. Phys. Chem. C* **2014**, *118*, 10481−10487.
(39) Wang, T.; Hu, X.; Dong, S. The fragmentation of gold nanoparticles induced by small biomolecules. *Chem. Commun.* **2008**, 4625−4627.
(40) Wu, H. P.; Huang, C. C.; Cheng, T. L.; Tseng, W. L. Sodium hydroxide as pretreatment and fluorosurfactant-capped gold nanoparticles as sensor for the highly selective detection of cysteine. *Talanta* **2008**, *76*, 347−352.
(41) Zhang, F. X.; Han, L.; Israel, L. B.; Daras, J. G.; Maye, M. M.; Ly, N. K.; Zhong, C. J. Colorimetric detection of thiol-containing amino acids using gold nanoparticles. *Analyst* **2002**, *127*, 462−465.
(42) Li, L.; Li, B. Sensitive and selective detection of cysteine using gold nanoparticles as colorimetric probes. *Analyst* **2009**, *134*, 1361−1365.
(43) Alarcos, N.; Cohen, B.; Ziolek, M.; Douhal, A. Photochemistry and Photophysics in Silica-Based Materials: Ultrafast and Single Molecule Spectroscopy Observation. *Chem. Rev.* **2017**, *117*, 13639−13720.
(44) Tira, D. S.; Focsan, M.; Ulinici, S.; Maniu, D.; Astilean, S. Rhodamine B-Coated Gold Nanoparticles as Effective "Turn-on" Fluorescent Sensors for Detection of Zinc II Ions in Water. *Spectrosc. Lett.* **2014**, *47*, 153−159.
(45) Chu, S.; Wang, H.; Ling, X.; Yu, S.; Yang, L.; Jiang, C. A Portable Smartphone Platform Using a Ratiometric Fluorescent Paper Strip for Visual Quantitative Sensing. *ACS Appl. Mater. Interfaces* **2020**, *12*, 12962−12971.
(46) Manjubaashini, N.; Kesavan, M. P.; Rajesh, J.; Thangadurai, T. D. Multispectroscopic and bioimaging approach for the interaction of rhodamine 6G capped gold nanoparticles with bovine serum albumin. *J. Photochem. Photobiol., B* **2018**, *183*, 374−384.
(47) Chandrakar, V.; Tapadia, K.; Gupta, S. K. Greener approach for gold nanoparticles synthesis from fruit peel extract of Manilkara zapota: a fluorometric assay for determination of thiourea. *Inorg. Nano-Met. Chem.* **2022**, 1−9.
(48) Prusti, B.; Chakravarty, M. An electron-rich small AIEgen as a solid platform for the selective and ultrasensitive on-site visual detection of TNT in the solid, solution and vapor states. *Analyst* **2020**, *145*, 1687−1694.
(49) Prasanth, S.; D Raj, R.; Vineeshkumar, T. V.; Thomas, R. K.; Sudarsanakumar, C. Exploring the interaction of L-cysteine capped CuS nanoparticles with bovine serum albumin (BSA): a spectroscopic study. *RSC Adv.* **2016**, *6*, 58288.
(50) Lim, I.-I. S.; Ip, W.; Crew, E.; Njoki, P. N.; Mott, D.; Zhong, C. J.; Pan, Y.; Zhou, S. Homocysteine-Mediated Reactivity and Assembly of Gold Nanoparticles. *Langmuir* **2007**, *23*, 826−833.
(51) Saroha, B.; Kumar, A.; Maurya, R. R.; Lal, M.; Kumar, S.; Rajor, H. K.; Bahadur, I.; Negi, D. S. Adsorption of cysteine on metal (II) octacynaomolybdate(IV) at different pH values: Surface complexes characterization by FT-IR, SEM with EDXA, CHNS and Langmuir isotherm analysis. *J. Mol. Liq.* **2022**, *349*, No. 118197.
(52) Hung, S. H.; Lee, J. Y.; Hu, C. C.; Chiu, T. C. Gold-nanoparticle-based fluorescent "turn-on" sensor for selective and sensitive detection of dimethoate. *Food Chem.* **2018**, *260*, 61−65.
(53) Link, S.; Sayed, M. A. E. Shape and size dependence of radiative, non-radiative and photothermal properties of gold nanocrystals. *Int. Rev. Phys. Chem.* **2000**, *19*, 409−453.
(54) Blatchford, C. G.; Campbell, J. R.; Creighto, J. A. Plasma Resonance − Enhanced Raman Scattering by Adsorbates on Gold colloids: the effects of aggregation. *Surf. Sci.* **1982**, *120*, 435−455.
(55) Wang, H.; Yang, L.; Chu, S.; Liu, B.; Zhang, Q.; Zou, L.; Yu, S.; Jiang, C. Semiquantitative Visual Detection of Lead Ions with a Smartphone via a Colorimetric Paper-Based Analytical Device. *Anal. Chem.* **2019**, *91*, 9292−9299.
(56) Jokerst, J. V.; Lobovkina, T.; Zare, R. N.; Gambhir, S. S. Nanoparticle PEGylation for imaging and therapy. *Nanomedicine* **2011**, *6*, 715−728.
(57) Lim, I.-I. S.; Mott, D.; Ip, W.; Njoki, P. N.; Pan, Y.; Zhou, S.; Zhong, C. J. Interparticle Interactions in Glutathione Mediated Assembly of Gold Nanoparticles. *Langmuir* **2008**, *24*, 8857−8863.
(58) Basu, S.; Pal, P. Glutathione-Induced Aggregation of Gold Nanoparticles: Electromagnetic Interactions in a Closely Packed Assembly. *J. Nanosci. Nanotechnol.* **2007**, *7*, 1904−1910.
(59) Zhang, L.; Xu, C.; Liu, C.; Li, B. Visual chiral recognition of tryptophan enantiomers using unmodified gold nanoparticles as colorimetric probes. *Anal. Chim. Acta* **2014**, *809*, 123−127.
(60) Feng, Y.; Liu, W.; Prieto, R. M.; Chen, X. D. Dye-protein interactions between Rhodamine B and whey proteins that affect the photoproperties of the dye. *J. Photochem. Photobiol., A* **2021**, *408*, No. 113092.
(61) Yuvaraj, P.; Ajantha, J.; Karuppusamy, M.; Easwaramoorthi, S.; Rao, J. R. Hydrogen Bond-Assisted Colorimetric Picomolar Level Detection of Hg^{2+} Ions in 100% Aqueous Solution. *ACS Sustainable Chem. Eng.* **2021**, *9*, 10309−10317.

https://doi.org/10.1021/acsomega.2c02725
ACS Omega 2022, 7, 29013−29026

(62) Benesi, H. A.; Hildebrand, J. H. A Spectrophotometric Investigation of the Interaction of Iodine with Aromatic Hydrocarbons. *J. Am. Chem. Soc.* **1949**, *71*, 2703−2707.
(63) Lodhi, M. S.; Khan, M. T.; Aftab, S.; Samra, Z. Q.; Wang, H.; Wei, D. Q. A novel formulation of theranostic nanomedicine for targeting drug delivery to gastrointestinal tract cancer. *Cancer Nanotechnol.* **2021**, *12*, No. 26.
(64) Andal, V.; Bhuvaneswari, G. Silver oxide nano-colloid based selective colorimetric sensor for the recognition of cystine in aqueous solution. *Mater. Res. Innovations* **2020**, *24*, 202−209.
(65) Pawlukojć, A.; Leciejewicz, J.; Ramirez-Cuesta, A. J.; Nowicka-Scheibe, J. L-Cysteine: Neutron spectroscopy, Raman, IR and ab initio study. *Spectrochim. Acta, Part A* **2005**, *61*, 2474−2481.
(66) Shtukenberg, A. G.; Hu, J.; Sahota, A.; Kahr, B.; Ward, M. D. Disrupting Crystal Growth through Molecular Recognition: Designer Therapies for Kidney Stone Prevention. *Acc. Chem. Res.* **2022**, *55*, 516−525.
(67) Claes, D. J.; Jackson, E. Cystinuria: mechanisms and management. *Pediatr. Nephrol.* **2012**, *27*, 2031−2038.

https://doi.org/10.1021/acsomega.2c02725
ACS Omega 2022, 7, 29013−29026